JOURNAL OF MATERIALS SCIENCE **37** (2002) 1237–1245

Mechanical and electrical properties of heavily drawn Cu-Nb microcomposites with various Nb contents

S. I. HONG
Department of Metallurgical Engineering, Chungnam National University, Taedok Science Town, Taejon 305-764, Korea
E-mail: sihong@hanbat.chungnam.ackr

M. A. HILL
Materials Science Division, Los Alamos National Laboratory, Los Alamos, NM 87545, USA

The mechanical and electrical properties of Cu-Nb filamentary microcomposite fabricated by the bundling and drawing process were examined. The strength increased gradually with increasing Nb content while the ductility was insensitive to Nb content. The ratios of yield stresses are found to be close to that of Young's moduli in various Cu-Nb microcomposites, suggesting that athermal obstacles primarily control the strength. The fracture morphologies show ductile fractures irrespective of Nb contents. Secondary cracking along the interfaces between subelemental wires was occasionally observed and the frequency of secondary cracking increased with increasing Nb content. The conductivity and the resistivity ratio ($\rho_{295\ K}/\rho_{75\ K}$) decreased with increasing Nb content. The decrease of the conductivity and the resistivity ratio can be explained by the increasing contribution of interface scattering.

1. Introduction

Deformation-processed Cu-based microcomposites incorporating a body-centered cubic (BCC) phase exhibit very high strengths with good electrical and thermal conductivities [1–8]. For such materials, the BCC phase such as Nb, Ta, Fe and Cr is initially present as primary dendrites in the copper matrix. Following extensive mechanical deformation of Cu-Nb, for example, niobium dendrites transform into fine niobium ribbons as a result of the ⟨110⟩ niobium texture upon drawing [1]. This microstructure contributes to the ultrahigh strength of Cu-Nb microcomposites. The strength of heavily deformed Cu-Nb exceeds that predicted by the rule-of-mixtures (ROM).

Since it requires heavy drawing to fabricate high strength wires, the diameter becomes usually too small for practical applications. The large diameter wire is desirable for magnet applications to avoid electrical breakdown and disintegration of the wire. One method to overcome this problem may be to bundle and bond many thin wires by drawing [9–12]. Spitzig *et al*. [13] noted that a 44% increase in strength of Cu-Nb could be obtained using a bundling and drawing process. This involves filling a container with small diameter wires and subsequently redrawing. Spitzig *et al*. [13], however, observed that on subsequent cold drawing of the bundled wires, the strength increased at a slower rate than that obtained on continuous cold drawing of the subelemental wire, and the strength differential decreased. They reported that upon subsequent cold drawing of the bundled wire to a diameter of 0.15 mm, the ultimate tensile strength is only 10% greater than that of the subelemental wire continuously drawn to the same diameter [13]. They suggested that a slow strengthening of bundled wire with total strain might result from a significant deterioration of the Nb filaments by heating and holding at 760°C during hot isostatic pressing and extrusion. The subelements from the bundling process can also debond and adversely affect mechanical properties if not processed optimally.

Previous studies have reported the increase of strength and the decrease of electrical conductivity with increasing Nb content [14, 15]. The increase of strength is thought to be associated with an increasing volume percentage of barriers (Nb filaments). Some researchers [15] studied the properties of Cu-Nb microcomposites with Nb contents less than 10% since they still exhibited favorable properties on a strength/conductivity basis. Spitzig *et al*. [15] reported that the ultimate strength of Cu-5 vol% Nb is significantly greater than that expected based on extrapolation from earlier work on higher Nb content alloys [14]. In this study, the physical properties of heavily drawn Cu-Nb microcomposites with various Nb contents were examined.

2. Experimental methods

Cu-Nb wires in this study were fabricated in collaboration with Ames Lab and Supercon. The processing procedure can be briefly described as follows. Cu-7.8 vol% Nb, Cu-10.4 vol%, Cu-12.9 vol% Nb and

Cu-15.6 vol% Nb were double consumable arc melted in an atmosphere of ultra high purity argon. Following the second melt, the ingot was 7.6 cm in diameter and 34.3 cm long. The ingots were subsequently machined to 6.4 cm in diameter for Cu-7.8 Nb, Cu-10.4 Nb and Cu-12.9 Nb and to 7.0 cm in diameter for Cu-15.6 Nb and canned in a copper can with a 7.6 cm outer diameter prior to extrusion. Because of these copper cans, the overall Nb contents for Cu-7.8 Nb, Cu-10.4 Nb, Cu-12.9 Nb and Cu-15.6 Nb were reduced to 5.5 vol%, 7.4 vol%, 9.2 vol% and 12.5 vol% respectively. The Cu-Nb was then extruded at 750°C to a 2.5 cm diameter rod and cold drawn to 1.5 mm. This corresponds to a logarithmic strain $\eta = 7.8$ (including a cold drawing strain of $\eta = 5.7$), where $\eta = \ln(A_o/A)$ and A_o and A are the original and final cross-sectional areas, respectively. The Cu-Nb drawn to 1.5 mm was bundled inside a copper can, hot isostatically pressed at 750°C at a pressure of 100 MPa, machined to a 7.6 cm diameter, and extruded to a 2 cm diameter. The previously deformation processed wires (to 1.5 mm) become sub-elements in a bundle and each bundled wire will be called subelemental wires hereafter. The extruded bundled wire was then swaged and drawn to achieve its final size of a 2 mm × 3 mm rectangular cross section. The logarithmic strain η after bundling is 6.63 including a cold drawing strain of $\eta = 3.96$. The total drawing strain including high temperature processing is therefore 11.76. The high temperature extrusion treatment is not as effective as cold drawing in refining the microstructure, thus this logarithmic strain cannot be directly compared with other studies [1, 2, 5–9]. The equivalent cold drawing strain was assumed to be 8.5–8.8 [13] for the comparison with other studies [5–9].

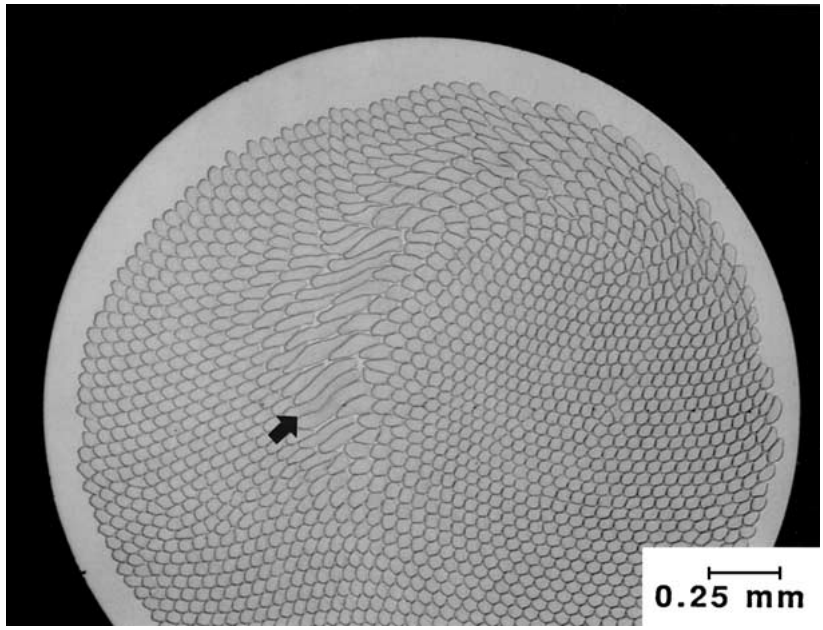

(a)

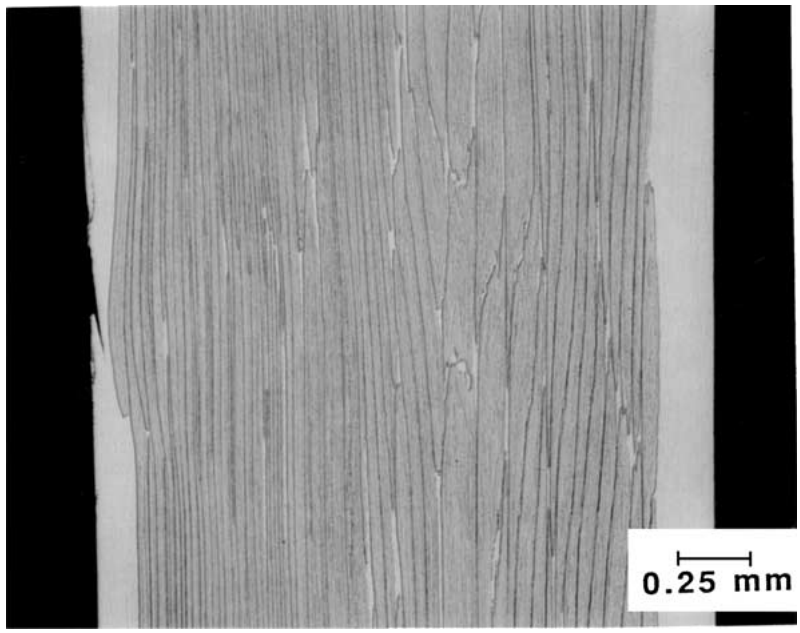

(b)

Figure 1 Optical micrographs showing the transverse and longitudinal sections of the as-drawn bundled Cu-12.5 vol% Nb wires.

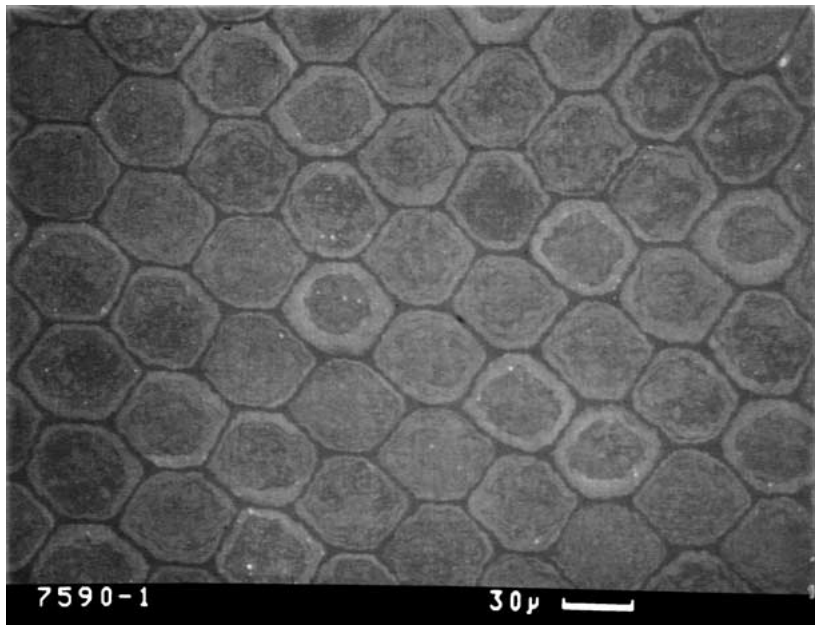

(a)

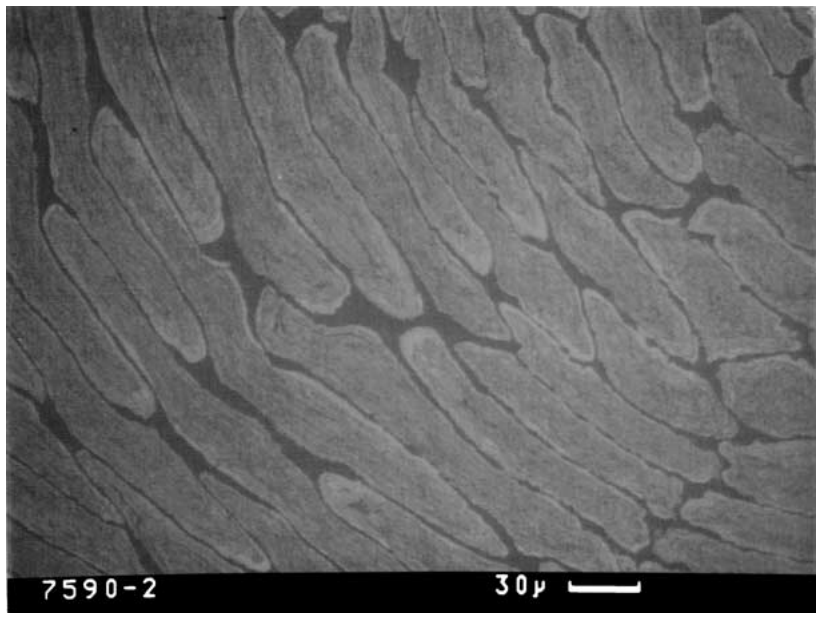

(b)

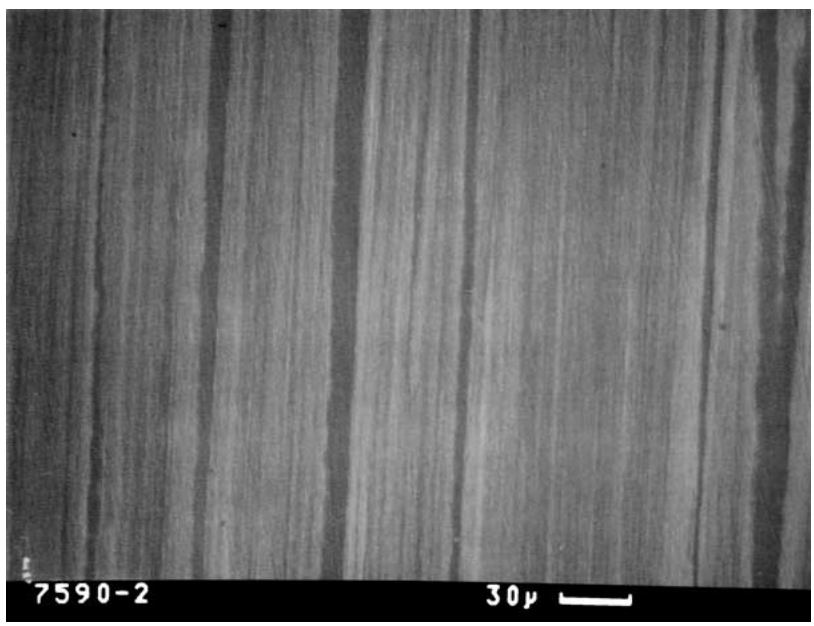

(c)

Figure 2 SEM micrograph showing the transverse (a, b) and longitudinal (c) sections. Note the hexagonal packing of subelemental wires in (a): See the text for details.

Tensile tests were performed in accordance with ASTM E8-93 on an MTS 880 testing machine at a strain rate of 1.67×10^{-3} sec^{-1} at room temperature. Fracture surfaces were examined using a Camscan SEM. TEM specimens were prepared by mechanically thinning followed by dimpling and ion milling on a liquid nitrogen stage. To ensure the samples were adequately cooled, the specimen rotation drive rod was submersed in liquid nitrogen for one hour prior to ion milling. TEM observations were carried out using a Phillips CM30 electron microscope operated at 300 kV. The resistivity was measured using a standard four-probe d.c. technique at room temperature, 295 K, and in a liquid nitrogen bath at 75 K.

3. Results and discussion

Fig. 1 shows the transverse and longitudinal sections of the as-drawn bundled Cu-Nb wires. The subelemental wire was originally round, but it becomes hexagonal in cross section for effective packing during bundling as shown in Fig. 1a. Occasionally the subelemental

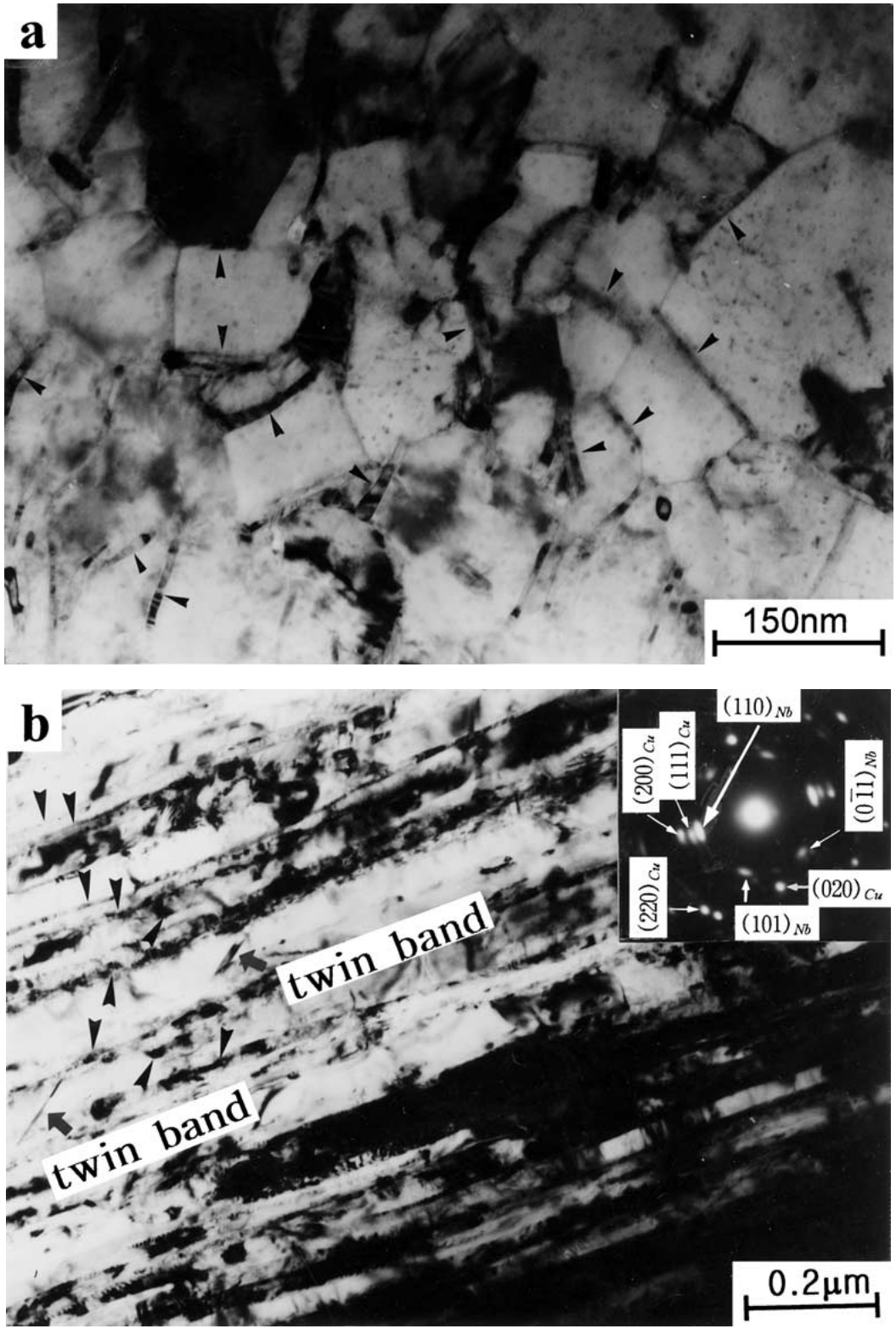

Figure 3 TEM micrographs showing the transverse and longitudinal sections of Cu-12.5 vol% Nb microcomposites.

wires have elongated cross sections, which are probably caused by local misalignment and bending during bundling and drawing. The SEM micrograph, in Fig. 2a, shows hexagonal packing of subelemental wires. Fig. 2b is a higher magnification micrograph of the region indicated by an arrow in Fig. 1a. The maximum width of elongated wires are approximately 30 μm, which is equal to the diameter of the subelemental wire. This indicates that the elongation in the cross section is due to local misalignment and bending. Fig. 2c is a SEM micrograph of the longitudinal section of bundled Cu-12.5 vol% Nb microcomposites at a higher magnification. In each subelemental wire, the filamentary structure resulting from aligned Nb fialments is apparent [10].

Fig. 3a and b are TEM micrographs showing the transverse and longitudinal sections of Cu-12.5 vol% Nb microcomposites. These figures show that Nb filaments (indicated by arrows) appear as thin and long plates with an average thickness of 14 nm and an average width of 179 nm. The cold drawing strain of bundled Cu-Nb, which may be a good estimate of the total cold work energy storage, is not readily available since the bundled Cu-Nb underwent complex intermediate thermo-mechanical processing. The total drawing strain of the bundled Cu-Nb, shown in Fig. 3, was suggested to be close to the cold drawing strain of 8–9 by Hong and Hill [10, 11] for the purpose of the comparison with other studies. Indeed, the thickness of Nb filaments (14 nm) in bundled Cu-Nb was found to be equal to the thickness of Nb filaments in Cu-Nb wire cold drawn to 8.5 [1]. Spitzig *et al.* [13] found that the morphology and size of Nb filaments did not change appreciably with Nb content in heavily drawn Cu-Nb wires. It is well known that the microstructure of heavily deformed Cu-Nb microcomposites is much finer than pure Cu processed in a similar manner because the recovery, and recrystallization cycle is effectively blocked by Nb filaments [1, 15].

The strength and ductility of various bundled Cu-Nb filamentary microcomposite wires at 75 K and 298 K are plotted as a function of Nb content in Fig. 4a and b. As shown in this figure, the strength increased with Nb content whereas the ductility remained relatively constant both at 75 K and 295 K. Fig. 5a and b show the fracture surfaces of Cu-12.5 vol% Nb at 295 K and 75 K at a lower magnification. As shown in these figures, secondary cracks due to debonding along the interface between subelemental wires were observed in some regions at both temperatures although they were more frequently observed at 295 K. The higher elongation at 295 K appears to be accompanied by more localized necking of subelemental wires. The more frequent debonding at 295 K may be due to a relatively large triaxial stress state caused by more localized necking of subelemental wires. Fig. 6a and b show the fracture surfaces of Cu-12.5 vol% Nb at 295 K and 75 K taken at a higher magnification in the region where no interfacial debonding was observed. These fractographs show ductile fractures at both temperatures. The dimple size in the original copper can was larger than that inside each subelemental wire, suggesting the microstructural scale in Cu-Nb subelemental wires is much finer than in the copper can.

The frequency of secondary cracking along the interfaces between subelemental wires increased with increasing Nb content. Fig. 7 shows the fracture surfaces of Cu-12.5 vol% Nb showing the secondary cracks along the interface between subelemental wires. This shows the tendency for necking of subelemental wires. If the stress developed perpendicular to the interface due to the localized deformation of subelemental wires is higher than the interfacial strength, debonding and the secondary cracking would develop. Therefore, secondary cracking would occur in some regions where the interfacial bonding strength is relatively weak. Spitzig *et al.* [16] reported that the dimple size in Cu-Nb decreased with increasing draw ratio in agreement with decreasing average spacing between Nb filaments. They [16] also reported that Nb filaments were evidently observed within the dimples. The observation of Spitzig *et al.* [16] suggests that cracks were likely to originate from Nb filaments. The insensitivity of the ductility of Cu-Nb microcomposites to Nb content as shown in Fig. 4 can be explained if the crack

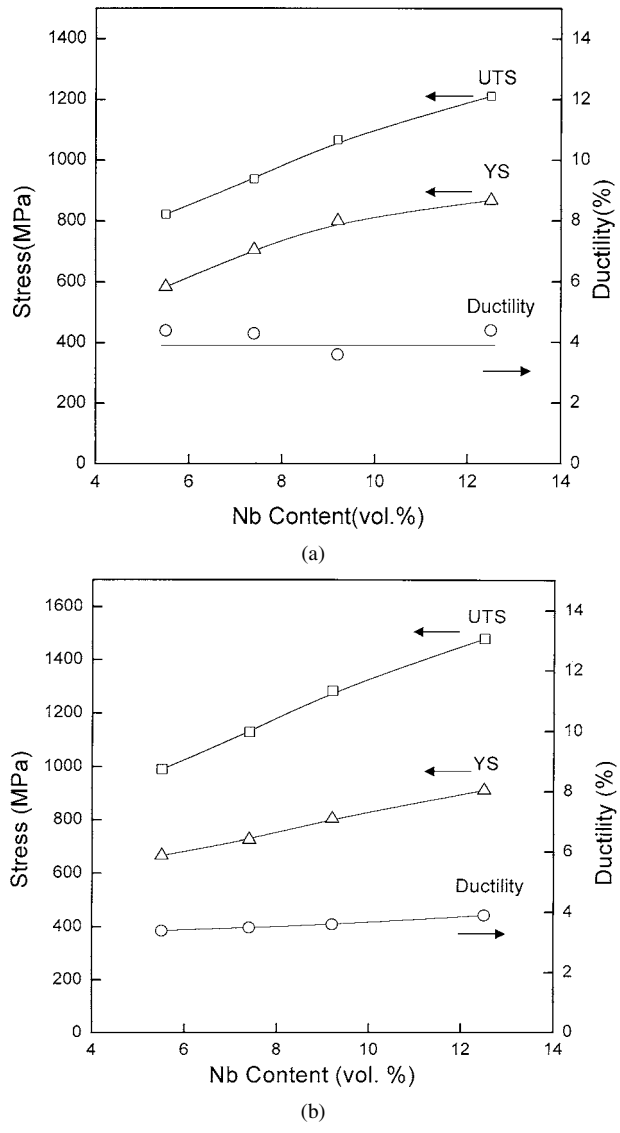

Figure 4 The strength and ductility of various bundled Cu-Nb filamentary microcomposite wires are plotted as a function of Nb content. (a) 295 K; (b) 75 K.

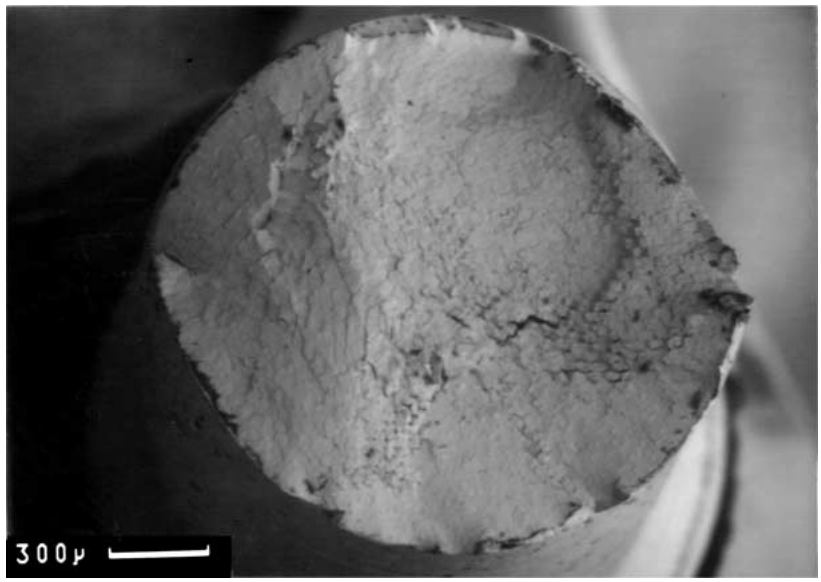

(a)

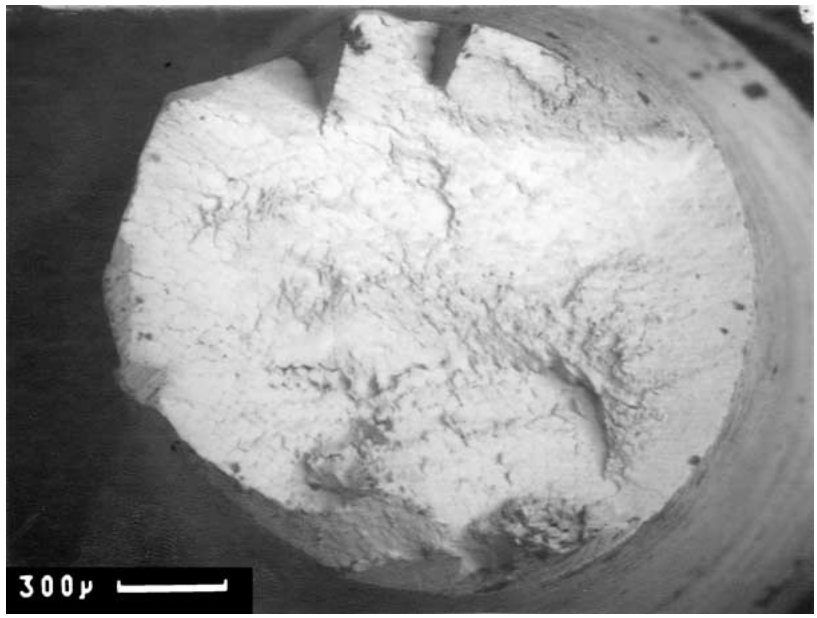

(b)

Figure 5 Fracture surfaces of Cu-12.5 vol% Nb at 298 K (a) and 77 K (b) at a lower magnification.

initiates from Nb filaments and the ductility of Cu-Nb wires is determined by the fracture strain of Nb filaments. Since the fracture strain of Nb filaments would remain the same in various Cu-Nb microcomposites at a given drawing strain, the ductility is insensitive to Nb content.

In Table I, the ratios of yield strengths (YS), ultimate tensile strengths (UTS) values and Young's moduli of as-drawn Cu-Nb wires at 295 K and 75 K are presented. Except Cu-5.5 Nb, the ratio of yield stresses (0.95–0.99) is close to that of Young's moduli (0.93), suggesting that the yield strength is primarily controlled by athermal obstacles [10, 17]. A slight decrease of the UTS ratio (0.82–0.83) is thought to be associated with an increasing contribution of thermal obstacles, such as dislocations during deformation [10, 17]. However, the observation that the ratio of UTS is still quite close to that of Young's moduli strongly indicates that athermal

TABLE I The ratios of yield strengths (Y.S.), ultimate tensile strengths (U.T.S.) and Young's moduli at 295 K and 75 K for as-drawn Cu-Nb wires

	295 K	75 K	Ratio (295 K/75 K)
Cu-5.5 Nb			
Y.S.	584 MPa	666 MPa	0.88
U.T.S.	822 MPa	990 MPa	0.83
Young's modulus	103 GPa	112 GPa	0.92
Cu-7.4 Nb			
Y.S.	706 MPa	725 MPa	0.97
U.T.S.	938 MPa	1129 MPa	0.83
Young's modulus	108 GPa	118 GPa	0.92
Cu-9.2 Nb			
Y.S.	799 MPa	803 MPa	0.99
U.T.S.	1067 MPa	1282 MPa	0.83
Young's modulus	110 GPa	125 GPa	0.88
Cu-12.5 Nb			
Y.S.	867 MPa	911 MPa	0.95
U.T.S.	1211MPa	1480 MPa	0.82
Young's modulus	124 GPa	134 GPa	0.93

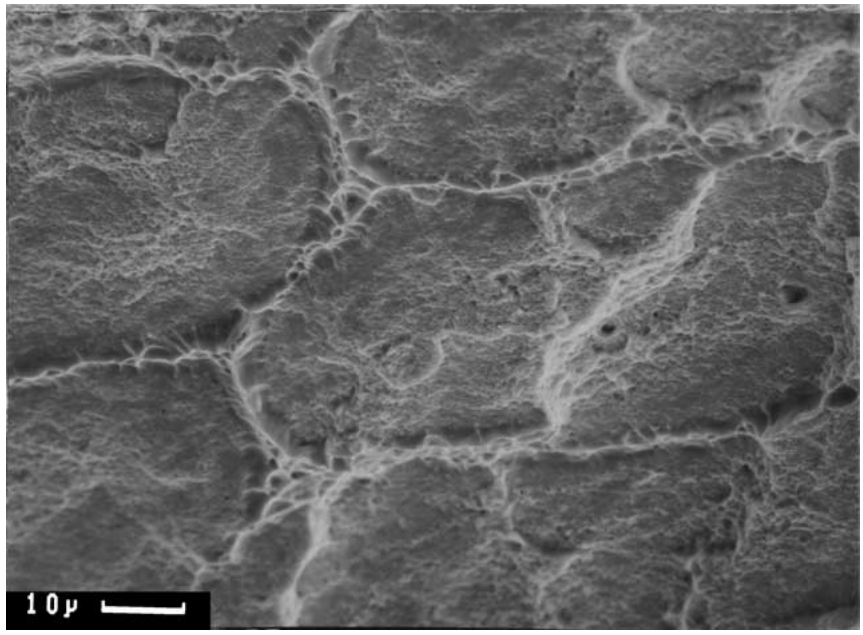

(a)

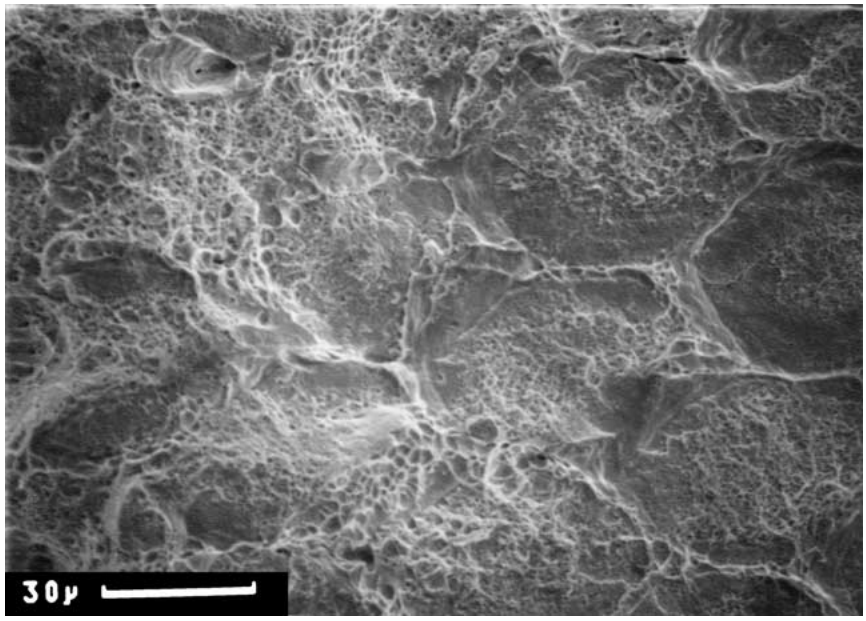

(b)

Figure 6 Fracture surfaces of Cu-12.5 vol% Nb at 298 K (a) and 77 K (b) taken at a higher magnification in the region where no interfacial debonding was observed.

obstacles are dominant barriers at the UTS. A slightly smaller YS ratio (0.88) for Cu-5.5 Nb than other Cu-Nb wires with higher Nb contents is thought to be due to lower volume percentage of Nb barriers [10, 17].

Fig. 8 shows the variation in electrical conductivity and the resistivity ratios at 295 and 75 K of Cu-Nb wires as a function of Nb content. The conductivity decreased with increasing Nb content although it decreased slowly at Nb contents higher than 8%. The resistivity ratios also decreased with increasing Nb content. The resistivity of Cu-Nb microcomposites can be partitioned into the contribution of various scattering mechanisms [18] as follows:

$$\rho_{\mathrm{Cu-Ag}} = \rho_{\mathrm{pho}} + \rho_{\mathrm{dis}} + \rho_{\mathrm{int}} + \rho_{\mathrm{imp}} \qquad (1)$$

where ρ_{pho} is the resistivity contribution from phonon scattering, ρ_{dis} is dislocation scattering, ρ_{int} is the interface scattering and ρ_{imp} is the impurity scattering. The contribution of the phonon scattering component, ρ_{pho}, is strongly temperature dependent [18]. On the other hand, the temperature dependence of the dislocation scattering, ρ_{dis}, and impurity scattering, ρ_{imp}, components does not depend on the type or concentration of lattice defects and can be ignored in materials with a stable microstructure and microchemistry [18]. The interface scattering can be temperature dependent if the interfacial spacing becomes comparable to or smaller than the mean free path of the electrons since the mean free path of electrons increases rapidly with a decrease in temperature [17]. Hong and Hill [19] reported that the change of the resistivity ratio ($\rho_{295\ \mathrm{K}}/\rho_{75\ \mathrm{K}}$) with heat treatment temperature showed the same trend as that of the conductivity.

Earlier, Karasek and Bevk [20] noted that electron scattering from dislocations and interfaces was particularly pronounced in composites with submicron

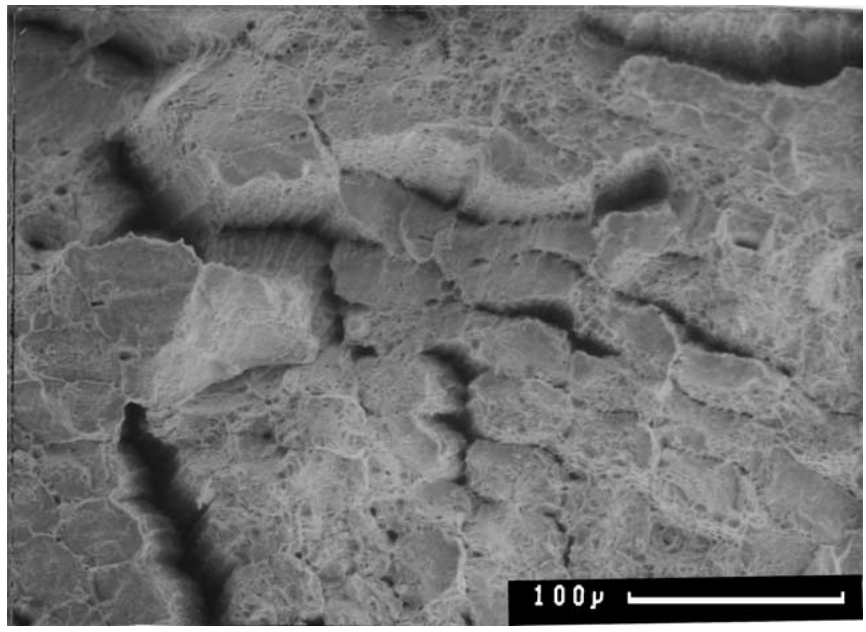

Figure 7 Feacture surfaces of Cu-12.5 vol% Nb showing the secondary cracks along the interface between subelemental wires.

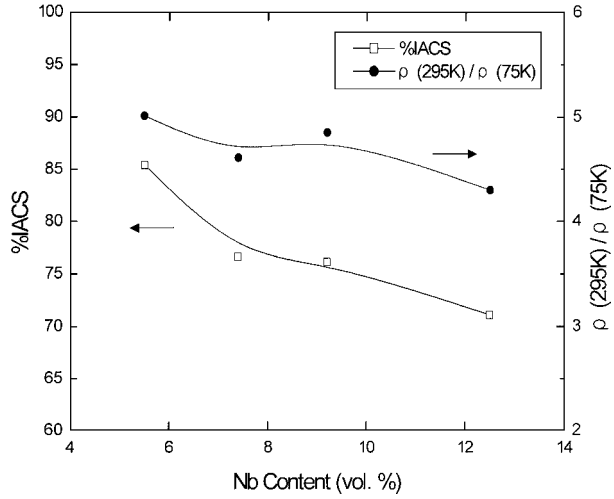

Figure 8 Variation in electrical conductivity and the resistivity ratios at 295 and 75 K of Cu-Nb wires as a function of Nb content.

filaments. They reasoned, however, that dislocation scattering in heavily deformed microcomposites may be the dominant scattering mechanism up to 300 K. Recent T.E.M. studies [21], however, have found that the dislocation densities at very high strains do not exceed $10^{11}/cm^2$. It is now known that the copper matrix undergoes dynamic recovery and recrystallization during room temperature drawing [16]. The observation that the filament spacing, filament thickness, and electrical conductivity decrease in proportion to wire diameter suggests that interface scattering is predominant in Cu-Nb microcomposites [18]. Based on detailed T.E.M. studies, Verhoeven *et al.* [18] suggested that resistivity in heavily drawn wire is mainly due to electron scattering at Cu-Nb interfaces and the increase in electrical conductivity following annealing is caused by the coarsening of niobium filaments. The decrease in the electrical conductivity with increasing Nb content is associated with an increasing fraction of Nb interfaces.

The decrease in the ratio of the resistivities ($\rho_{295\ K}/\rho_{75\ K}$) with increasing Nb content can also be explained by the increasing contribution of interface scattering. If the contribution of phonon scattering is high, the ratio of the resistivities ($\rho_{295\ K}/\rho_{75\ K}$) is usually high [18]. The mean free path of electrons at low temperatures is comparable to or larger than the microstructural scale (i.e. interfacial spacing) and increases rapidly with a decrease in temperature. The mean free path of electrons in copper at room temperature is about 40 nm [18]. The mean free path in copper at 75 K was reported to be approximately 140 nm [22], which is comparable to the average width of the Cu matrix. Hong [23] suggested that the width of Cu matrix, λ, between Nb filaments can be given by the following equation:

$$\lambda = L/2 - t = (0.065wt/V_f)^{1/2} - t \qquad (2)$$

where V_f is the volume fraction of Nb filaments, w is the width of Nb filaments and t is the thickness of Nb filaments. The inter-filamentary spacing, λ, calculated using the above equation decreases with increasing Nb content and it becomes smaller than 140 nm, the mean free spacing at 75 K, above 9.2 vol% Nb. This may result in the increase of the resistivity at 75 K in Cu-12.5 vol% Nb and the rapid decrease of the resistivity ratio ($\rho_{295\ K}/\rho_{75\ K}$) at high Nb contents.

4. Conclusions

Based upon a study of the strength and ductility of heavily drawn bundled Cu-Nb filamentary microcomposites, the following conclusions can be drawn.

1. The strength increased gradually with increasing Nb content while the ductility was insensitive to Nb content. The fracture morphologies show ductile fractures irrespective of Nb contents. The frequency of secondary cracking along the interfaces between subelemental wires increased with increasing Nb content.

2. The ratios of yield stresses are found to be close to that of Young's moduli in various Cu-Nb microcomposites, suggesting that athermal obstacles primarily control the strength.

3. The conductivity and the resistivity ratio ($\rho_{295\ K}/\rho_{75\ K}$) decreased with increasing Nb content. The decrease of the conductivity and the resistivity ratio can be explained by the increasing contribution of interface scattering.

Acknowledgments

The authors acknowledge support of the United States Department of Energy (W7405-ENG36), the National Science Foundation, and the Korea Science and Engineering Foundation (971-0803-034-2). We express appreciation for the collaboration of our colleagues P. Papin, R. Aikin, J. Montoya, and M. Hundley of LANL and J. S. Song, M. S. Lim, and J. H. Ahn of CNU. The authors are grateful to Dr. Don Parkin (CMS/LANL) for his support and encouragement.

References

1. J. D. VERHOEVEN, L. S. CHUMBLEY, F. C. LAABS and W. A. SPITZIG, *Acta Metall. Mater.* **39** (1991) 2825.
2. P. D. FUNKENBUSCH and T. H. COURTNEY, *Scripta Metall.* **23** (1989) 1719.
3. T. H. COURTNEY, in "Metal Matrix Composites: Processing and Interfaces," edited by R. K. Everett and R. J. Arsenault (Academic Press, San Diego, USA, 1991) p. 101.
4. C. L. TRYBUS and W. A. SPITZIG, *Acta Metall.* **37** (1989) 1971.
5. W. A. SPITZIG, C. L. TRYBUS and J. D. VERHOEVEN, in "Metal Matrix Composites: Mechanisms and Properties," edited by R. K. Everett and R. J. Arsenault (Academic Press, San Diego, USA, 1991) p. 151.
6. P. D. FUNKENBUSCH and T. H. COURTNEY, *Scripta Metall. Mater.* **24** (1990) 1175.
7. C. BISELLI and D. G. MORRIS, *Acta Metall. Mater.* **42** (1994) 163.
8. *Idem.*, *ibid.* **44** (1996) 493.
9. U. HANGEN and D. RAABE, *ibid.* **43** (1995) 4075.
10. S. I. HONG and M. A. HILL, *ibid.* **46** (1998) 4111.
11. *Idem.*, *Mater. Sci. Eng.* A **281** (2000) 189.
12. S. I. HONG, *Scripta Mater.* **39** (1998) 1685.
13. W. A. SPITZIG, F. C. LAABS, H. L. DOWNING and C. V. RENAUD, *Materials and Manufacturing Processes* **7** (1992) 1.
14. J. BEVK, J. P. HARBISON and J. L. BELL, *J. Appl. Phys.* **49** (1978) 6031.
15. W. A. SPITZIG, H. L. DOWNING, F. C. LAABS, E. D. GIBSON and J. D. VERHOEVEN, *Metall. Trans.* **24A** (1993) 7.
16. W. A. SPITZIG, A. R. PELTON and F. C. LAABS, *Acta Metall.* **35** (1987) 2427.
17. S. I. HONG and M. A. HILL, *Scripta Mater.* **42** (2000) 737.
18. J. D. VERHOEVEN, H. L. DOWING, L. S. CHUMBLEY and E. D. GIBSON, *J. Appl. Phys.* **65** (1989) 1293.
19. S. I. HONG and M. A. HILL, *Mater. Sci. Eng.* A **264** (1999) 151.
20. K. R. KARASEK and J. BEVKM, *J. Appl. Phys.* **52** (1981) 1370.
21. C. L. TRYBUS, L. S. CHUMBLY, W. A. SPITZIG and J. D. VERHOEVEN, *Ultramicroscopy* **22** (1989) 315.
22. G. FROMMEYER and G. WASSERMANN, *Phys. Stat. Sol.* A **27** (1975) 99.
23. S. I. HONG, *J. Mater. Res.* **15** (2000) 1889.

Received 21 September 2000
and accepted 2 November 2001